utility of considering a post-treatment by ICA for signals separation. For the period 2003–2008, we present correlation (Fig. 3) and RMS (Fig. 4) maps computed between the ICA400 (respectively ICA500) and Gaussian-filtered solutions with a radius of 400 km (500 km), named in the followings G400 (G500). High correlation coefficients are generally observed over land (greater than 0.9), increasing with the smoothing radius, especially over areas with large hydrological signals, *i.e.*, Amazon, Congo and Ganges basins, boreal regions. On the contrary, low correlation values, structured as stripes, are located over arid and semi-arid regions (southwest of the US, Sahara, Saudi Arabia, Gobi desert, centre of Australia), especially for GFZ and JPL solutions. These important RMS differences between Gaussian and ICA-based solutions reveal that the GRACE signals still contains remaining stripes after the Gaussian filtering. This justifies that extracting the useful continental hydrology signals requires a further processing. For this purpose, ICA succeeds in isolating this noise in its second and third components (as illustrated in Fig. 1).

In Fig. 4, we observe that the spatial distribution of the RMS between ICA solutions and Gaussian solutions presents north–south stripes with values generally lower than 30 mm, except for some spots between ± (20–30)° of latitudes on the GFZ (Fig. 4c, d) and JPL (Fig. 4e, f) solutions. The ICA approach allows the filtering of remnant stripes present in the Gaussian solutions, especially for GFZ and JPL (Fig. 4c to f). These unrealistic structures (stripes and spots), which correspond to resonances in the orbit of the satellites, are clearly filtered out using the ICA approach (compare with Fig. 1). A more important smoothing due to a larger radius caused a decrease of the RMS between ICA and Gaussian solutions (Fig. 4a, c, e). The RMS can reach 100 mm between ICA400 and G400 and only 65 mm between ICA500 and G500 for the GFZ solutions.

4.2.2. ICA versus destriped and smoothed solutions

Similar to Figs. 3 and 4, we present correlation (Fig. 5) and RMS (Fig. 6) maps over the period 2003–2008; between ICA400 (ICA500 respectively) and destriped and smoothed solutions with radii of 300 km (DS300) and 500 km (DS500), made available by Chambers (2006). The correlation maps between ICA400 (respectively ICA500) and DS300 (DS500) exhibit very similar patterns compared with those presented in Fig. 3, except in the McKenzie Basin and Nunavut (northern Canada) where low correlation or negative correlations for GFZ and JPL solutions (Fig. 5c to f) are found.

The RMS differences between ICA and destriped and smoothed solutions present low values above 30° (or below −30°) of latitude (<30 mm of EWT), with the exceptions of Nunavut in northern Canada and extreme values (up to 100 mm) in the tropics. This is clearly due to the low performance of the destriping method in areas close to Equator as previously mentioned by Swenson and Wahr (2006) and Klees et al. (2008). These extrema are especially present in the DS300 GFZ and JPL solutions. Some secondary maxima (up to 80 mm) are also noticed for the GFZ and the JPL solutions. These important differences correspond to north–south stripes that still appear in the destriped and smoothed solutions despite the filtering process (and that can be filtered out by applying an ICA approach — see the results for DS300 GFZ solution of March 2006 in Fig. 7). For an averaging radius of 500 km, the RMS between ICA500 and DS500 is lower than 20 to 30 mm, except for the Nunavut (Fig. 6b, d, f), along the Parana stream (40 to 50 mm in the CSR solutions — Fig. 6b), and along the Amazon and Parana streams (60 to 80 mm in the GFZ solutions — Fig. 6d).

These low spatial correlations suggest Gaussian–ICA provides at the least equivalent results on the continents to the smoothing–destriping method. Besides, it is interesting that both approaches are based on a pre-Gaussian filtering. Short wavelength differences between the maps obtained separately using ICA and destriping reveals the limitation of the destriping which generates artefacts in the tropics.

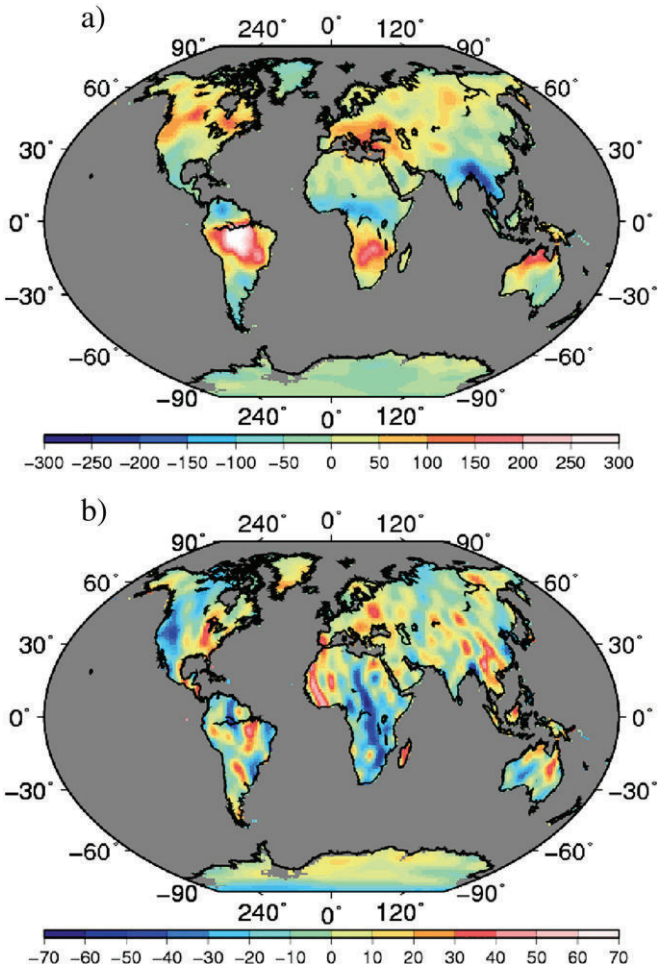

Fig. 7. GRACE water storage from GFZ destriped and smoothed with a Gaussian filter of 300 km of radius for March 2006. (Top) First ICA component corresponding to land hydrology. (Bottom) Sum of the second and third components corresponding to the north–south stripes.

4.2.3. Trend comparisons

The effects of the stripes on the trends estimated using GRACE-based TWS is supposed to be significant. From the time series of TWS anomaly grids derived from GRACE (using Eq. 1), the temporal trend, seasonal and semi-annual amplitudes were simultaneously fitted by least-square adjustment at each grid point over the period 2003–2008 (see Frappart et al., in press, for details). We present in Fig. 8 trends of TWS for ICA400 (Fig. 8a) and ICA500 (Fig. 8b), for G400 (Fig. 8c) and G500 (Fig. 8d), and for DS300 (Fig. 8e) and DS500 (Fig. 8f).

The trend estimates exhibit large differences in spatial patterns and the amplitude of the signal, especially between ICA and other processing methods. The most significant differences over land (except Antarctica) are located at high latitudes, over Scandinavia, and the Laurentide region, in the northeast of Canada. The ICA400 and ICA500 solutions present negative trends of TWS (Fig. 8a, b), whereas the G400 and G500 and the DS300 and DS500 present large positive trends (Fig. 8c to f). These two zones are strongly affected by the post-glacial rebound (PGR) which has a specific signature in the observed gravity field. This effect accounts for positive trends in these regions. According to the PGR models developed by Peltier (2004) and Paulson et al. (2007), its intensity can be greater in these regions than the trends measured by GRACE. For example, in the Nelson Basin, Frappart et al. (in press) found a trend of TWS from GRACE of (4.5 ± 0.2) mm/yr over 2003–2006, while model-based estimates of PGR represents 18.8 mm/yr in this region. As the space and time characteristics of the glacial isostatic adjustment (GIA) is different than the one from

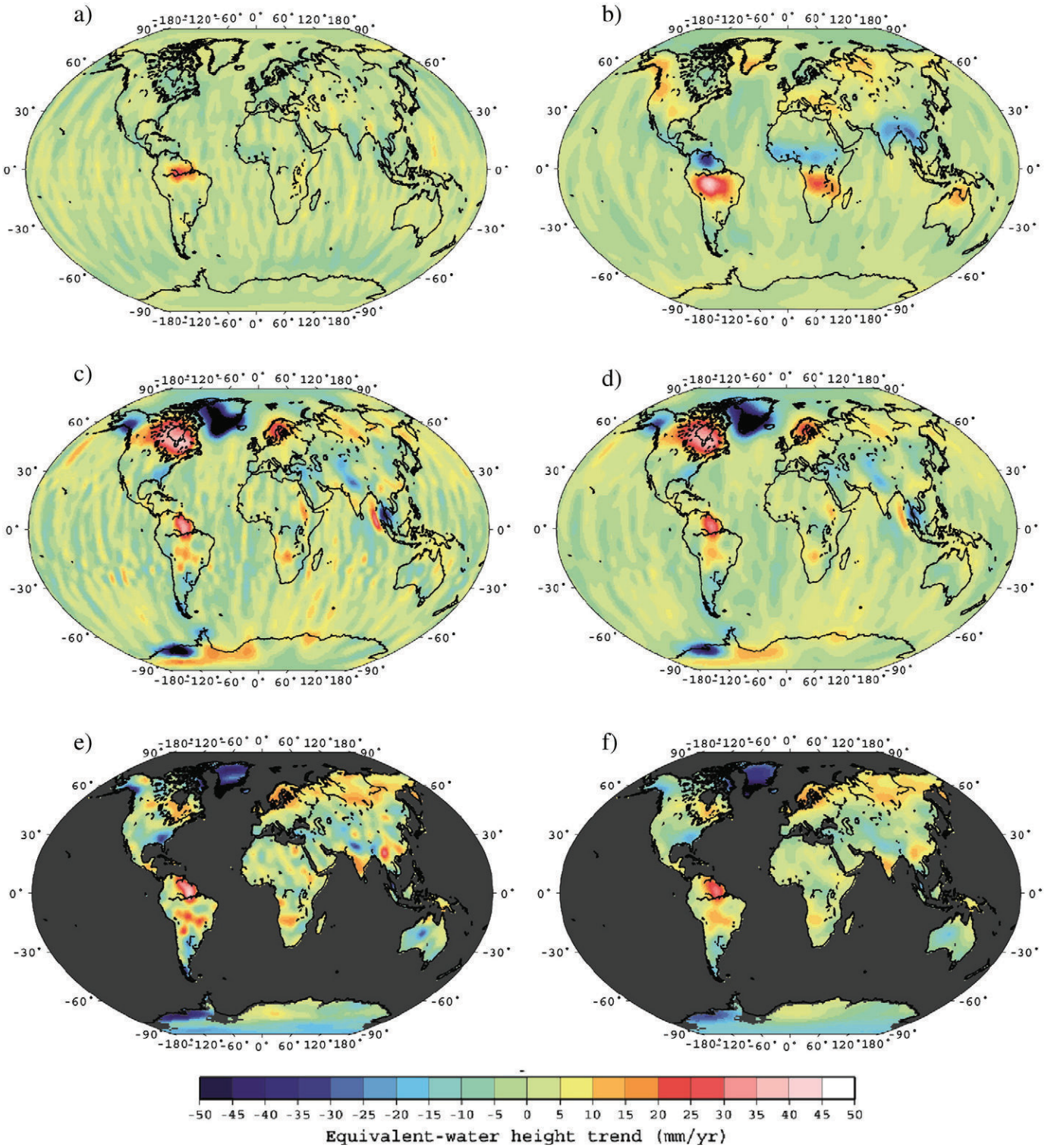

Fig. 8. Trend maps over the period 2003–2008 of TWS using the GFZ solutions a) ICA400, b) ICA500, c) G400, d) G500, e) DS300 and f) DS500.

continental hydrology, the ICA approach may have separated it from the signals only related to the redistribution of water masses. Unfortunately, trends computed on the 2nd and 3rd ICs, and their sum does not exclusively correspond to GIA, but to a mixture of geophysical remaining signals and noise. It is also worth noticing that the gravity signature of the Sumatra event in December 2004, which is clearly apparent on the Gaussian-filtered solutions (Fig. 8c, d), is not visible in the 1st mode of the ICA solutions (Fig. 8a, b), but is present in the sum of the 2nd and 3rd ICs. This confirms that the ICA is able to isolate a pure hydrological mode in the GRACE products.

A second important difference between ICA solutions and Gaussian-filtered and destriped and smoothed solutions concerns the impact of the filtering radius on the trends estimate. An increase of the filtering radius causes a smoothing of the solutions, and, consequently, a decrease of the intensity of the trends on Gaussian-filtered and destriped and smoothed solutions (Fig. 8c to f). On the contrary,

the intensity of the trends increases with the radius of prefiltering on the ICA solutions. The location of the extrema is also shifted. This change in the location is a side-effect of the prefiltering with the Gaussian filter. A better location of the trends is observed when a Gaussian-filter of 400 km of radius is used instead of 500 km (see for instance the trends pattern in the Amazon and Orinoco Basins in Fig. 8a, b).

4.3. Basin-scale comparisons

Changes in total water volume were estimated for 27 drainage basins whose locations are shown in Fig. 9 (the corresponding areas are given in Table 1). ICA400 and ICA500 were used to compute regional TWS averages versus time (Eqs. 8 and 9). These time series were compared to the G400 and G500, and the DS300 and DS500 respectively. Examples of the Amazon, the Ob and the Mekong basins for ICA400, G400 and DS300 (GFZ solutions) are presented in Fig. 10. TWS exhibit very similar temporal patterns for all the types of filtering radii and basins. The correlation coefficients between the ICA and the Gaussian-filtered, or the ICA and the destriped and smoothed time series of TWS are greater than 0.9 for 21 out of 27 basins. For five other basins (Amur, Colorado, Hwang Ho, Parana, and St Lawrence), most of the correlation coefficients are greater than 0.8 or 0.9, and the others (generally the correlation coefficients between ICA and destriped and smoothed GFZ solutions) greater than 0.65 or 0.7. The only exception is the McKenzie Basin where all the correlation coefficients between ICA and destriped and smoothed are lower than 0.75 ($r_{(ICA400,DS300)\ JPL} = 0.45$ and $r_{(ICA500,DS500)\ JPL} = 0.51$). For the GFZ solutions, some unrealistic peaks are present in the destriped and smoothed TWS time series for some periods (Fig. 10a, b, c). These peaks only appear on the Gaussian-filtered solutions for the smallest basins, such as the one of the Mekong river (Fig. 10c), but are not present in the ICA-filtered solutions. RMS difference between ICA-filtered solutions and the other type of solutions are generally lower than 30 mm of equivalent water height and logically decrease with the radius of filtering. Differences with the ICA solutions are generally larger for the GFZ-based destriped solutions, especially in tropical regions where the performances of the destriping are not the best and the hydrological signal the largest (Fig. 11).

Table 1
The 29 drainage basins considered in this study sorted by decreasing area.

Number	River basin	Area (10^6 km²)
1	Amazon	6.20
2	Amur	1.88
3	Brahmaputra	0.65
4	Colorado	0.63
5	Congo	3.81
6	Danube	0.81
7	Dniepr	0.52
8	Euphrates	0.81
9	Ganges	0.97
10	Hwang Ho	0.74
11	Lena	2.45
12	McKenzie	1.73
13	Mekong	0.77
14	Mississippi	3.32
15	Niger	2.18
16	Nile	3.16
17	Ob	2.84
18	Okavango	0.83
19	Orinoco	0.87
20	Parana	2.98
21	St Lawrence	1.12
22	Tocantins	0.86
23	Volga	1.42
24	Yangtze	1.78
25	Yenisey	2.56
26	Yukon	0.82
27	Zambezi	1.39

We present an analysis of possible sources of error on the computation of regional averages versus time using the 300, 400, 500-km pre-filtered ICA solutions. This task is made on the longest available period of time for each centre (CSR, JPL, and GFZ), and for the 27 drainage basins (Table 1).

The formal error decreases with the number of points (see Eqs. 10 and 11), the surface of the considered region, and the value of error σ_k at each grid point. In the case of the Amazon Basin (~6 million of km²), the formal error is only of 4.5 mm when $\sigma_k = 100$ mm of equivalent water height. For the Dniepr river basin that represents the smallest surface of our chosen basins (~0.52 million of km²), the formal error

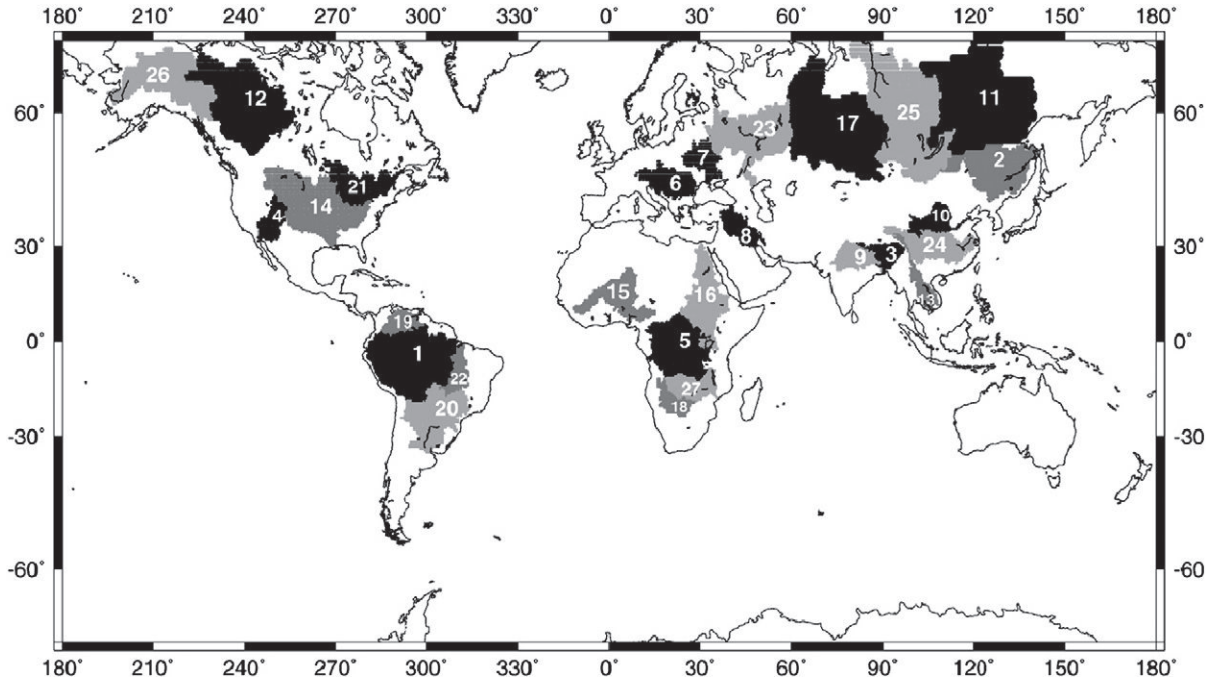

Fig. 9. Location of the 27 drainage basins chosen in this study. See Table 1 for the correspondence between basins and numbers.

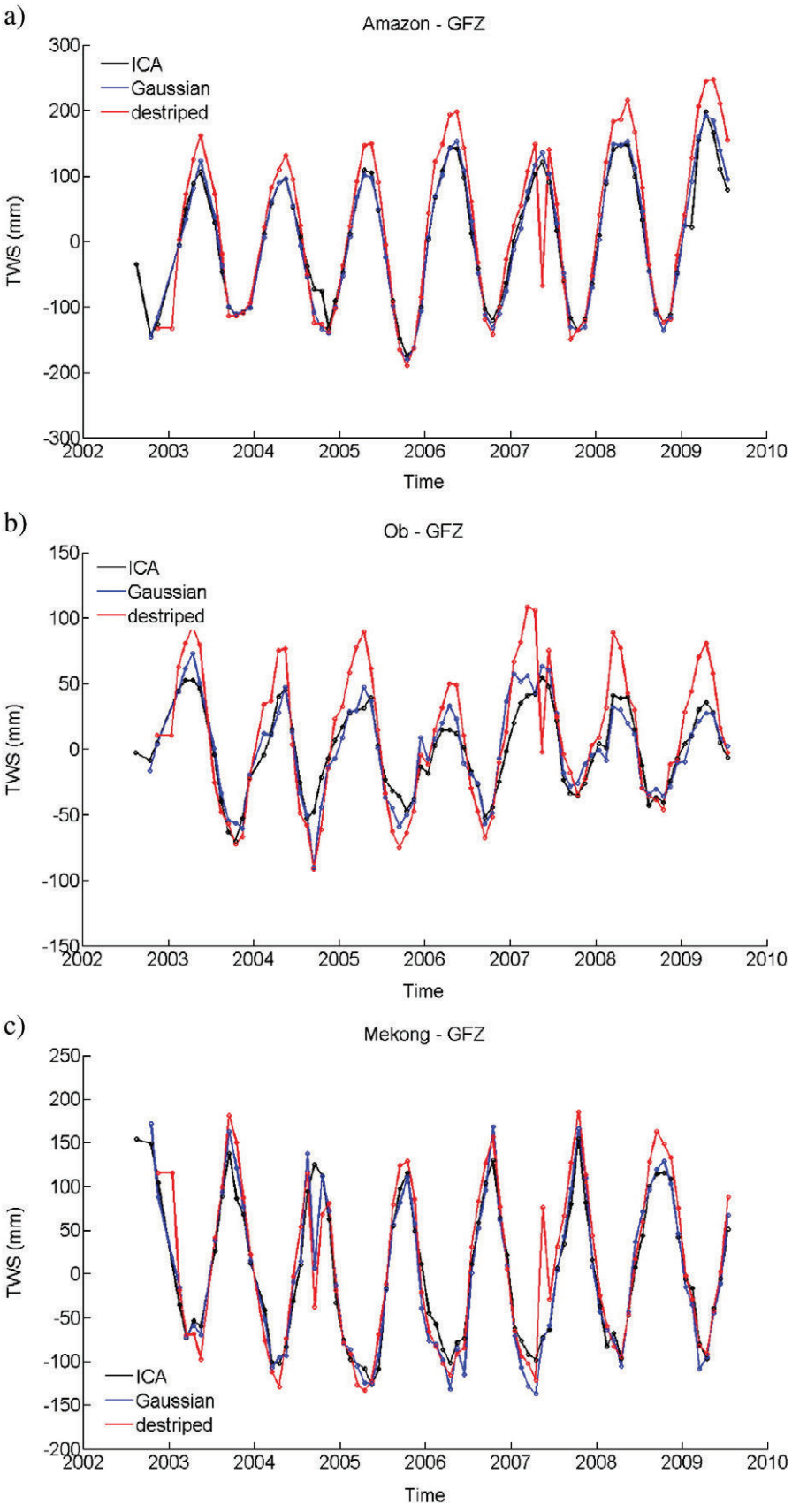

Fig. 10. Time series of TWS (mm) derived from ICA400 (black), G400 (blue), DS300 (red) for GFZ solutions over the Amazon (a), Ob (b) and Mekong (c) basins.

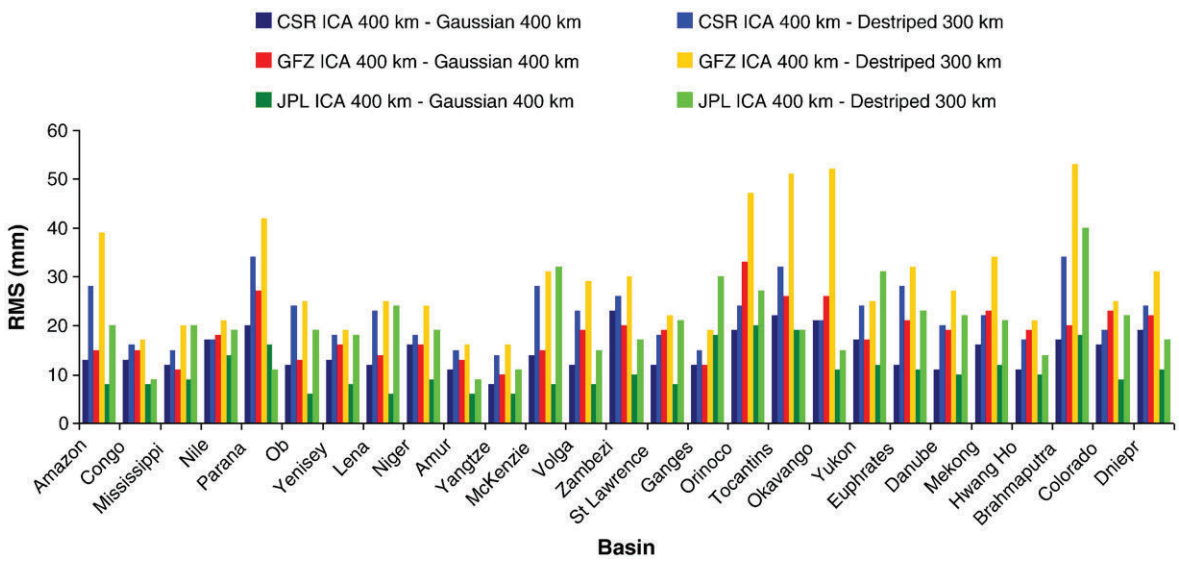

Fig. 11. RMS between ICA400 and G400 for CSR (dark blue), GFZ (red), and JPL (dark green) solutions and between ICA400 and DS300 for CSR (light blue), GFZ (orange), and JPL (green) solutions per basin (sorted by decreasing area of drainage basin) over the period October 2002–July 2009.

reaches 12.3 mm. For the series of basins, the maximum values of formal errors on the regional average are in the range of 10–15 km^3 of water volume per hundred of mm of error on the gridded points.

To estimate the frequency cut-off error or "omission error", we made statistics of the numerical tests which were performed to see what maximum error can be reached using Eq. (12). We computed this residual quantity for 300, 400 and 500 km-filtered ICA solutions and for each hydrological basin for $N_1 = 60$ and $N_2 = 300$. The maximum error is always less than 1 km^3, as shown previously (Ramillien et al., 2006a), and it decreases with the filtering wavelength of the pre-processing. In other words, this error simply increases with the level of noise in the data. For the 300 km and 400 km pre-filtered solutions, the maximum values are found for the Amur River: 0.3 km^3 (CSR), 0.1 km^3 (JPL), and 0.8 km^3 (GFZ), and 0.04 km^3 (CSR), 0.09 km^3 (JPL), 0.08 km^3 (GFZ) respectively. While using the 500-km-filtered solutions, the error of truncation is less than 0.005 km^3.

The leakage error on the ICA solutions was computed per drainage basin (see Section 3.5). The results are presented in Fig. 12 for the different centres and radii of Gaussian prefiltering of 300, 400 and 500 km. We observed that the leakage decreases with the radius of filtering and is generally lower in the JPL solutions, which presents lowest peak-to-peak amplitudes. This leakage error is logically greater in areas where several basins with large hydrological signal are close, *i.e.*, South America with the Amazon, the Parana, the Orinoco and the Tocantins, or tropical Asia with the Ganges, the Brahmaputra and the Mekong rivers. The leakage error is also greater for basins with small hydrological signals close to a predominant basin having important hydrological variations, *i.e.*, the Okavango and the Zambezi with the Congo.

4.4. Basin-scale validation

GRACE observations were used to estimate variations in TWS over the Murray–Darling Basin (see Fig. 13 for the location of the basin) at an interannual scale from January 2003 to December 2008. The annual variations in TWS from GRACE for different types of solutions were compared to the annual TWS computed as the sum of *in situ* observations (SW + GW) and NOAH outputs (SM). In the Murray–Darling River basin, GLDAS–NOAH simulations of SM range from 5 to 29% (in volumetric water content) across the basin for the study

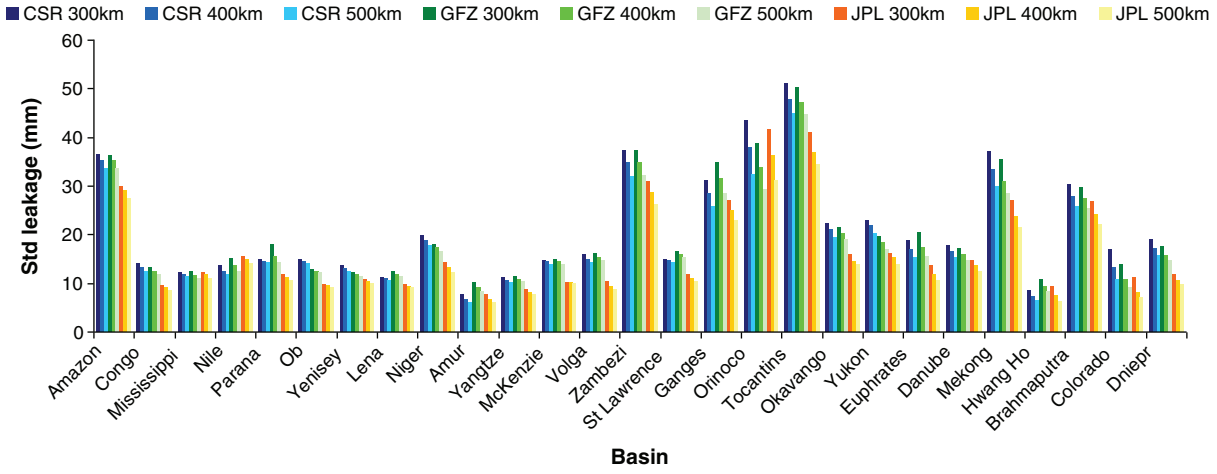

Fig. 12. Standard deviation of the leakage error (mm) per basin (sorted by decreasing area of drainage basin) over the period October 2002–July 2009 for the ICA solutions.

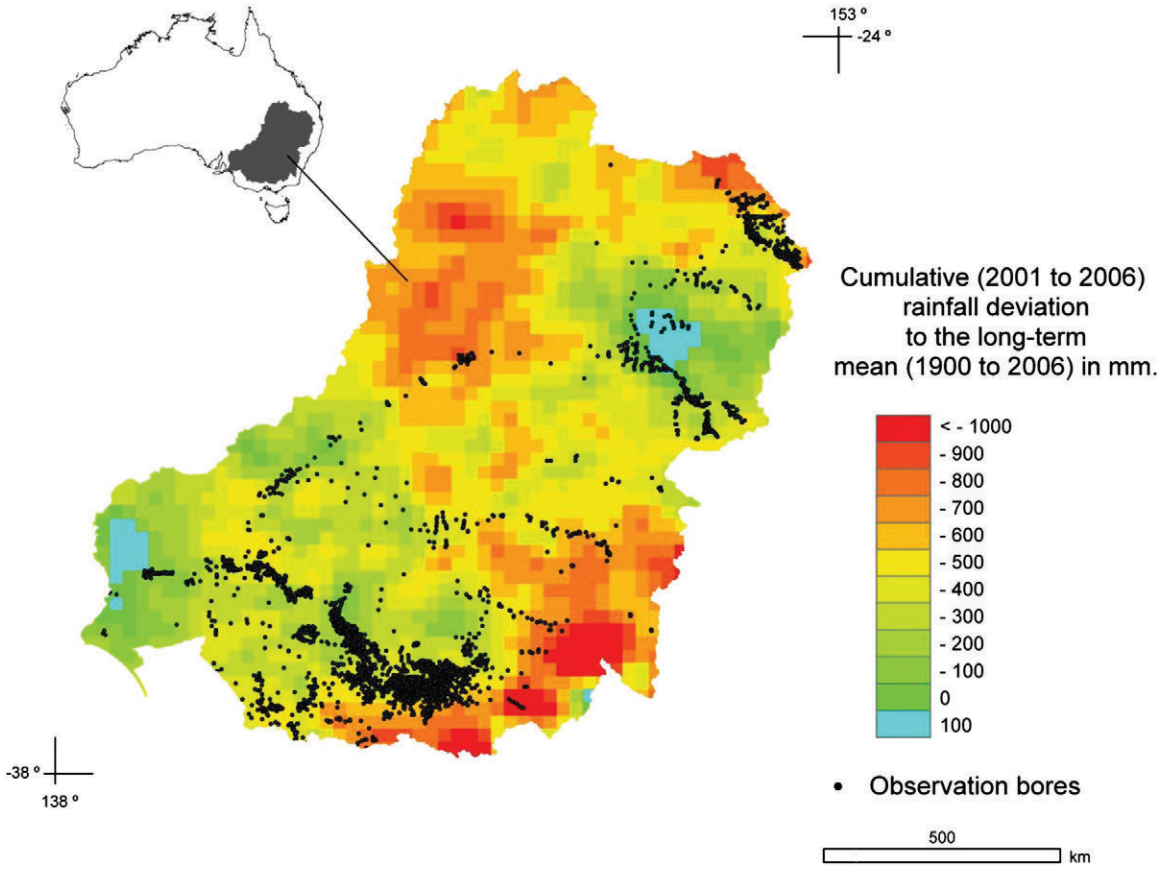

Fig. 13. Map of the Murray–Darling drainage basin in Australia. Cumulative rainfall deficit across the Murray–Darling Basin for the 2001–2006 period and location of the shallow groundwater monitoring bores.

period, and are within typical values for monthly means at 1° resolution (Lawrence & Hornberger, 2007). Besides, Leblanc et al. (2009) show that, between 2003 and 2007, the linear rate of water changes for the GRACE TWS time series is similar to that observed for the annual total water storage from *in situ* observations and modeling. The combined annual anomalies of surface water, groundwater and soil moisture are highly correlated with the annual GRACE TWS ($R = 0.94$ and mean absolute difference $= 13$ km^3 for the 2003–2007 period). These latter interannual field-based data are considered as the reference in the following analysis. The results are presented on Fig. 14 for the GFZ solutions. The ICA solutions generally present a temporal pattern closer to the so-called reference (*i.e.*, the sum of *in situ* data for SW and GW and model outputs for SM). This temporal pattern and the associated dynamics do not change with the radius of filtering, which is not the case with the Gaussian-filtered, and the destriped and smoothed solutions. None of the solutions are able to retrieve the minimum observed in 2007 in the reference dataset. It is important to notice that the largest part of the interannual variations of TWS comes from the GW reservoir. For this hydrological component, the water storage is derived from *in situ* measurements through Eq. (1), and is highly dependent on the specific yield coefficient; where averages of local measurements are used to determine ranges of regional-scale estimates. For the Murray–Darling Basin, composed of several aquifers, this leads to a broad range of spatial variability for the GW estimates. This variability is around or greater than 20 km^3 for 2002, 2007 and 2008 and around 10 km^3 for 2003, 5 km^3 in 2004 and 2006, 2.5 km^3 in 2005. We present yearly deviations to the reference for the different considered solutions (Fig. 15) over 2003–2006, where the range of variability of the GW is lower. Generally, the absolute deviation of ICA-derived TWS to the reference is lower than 5 km^3, especially for solutions filtered at 400 km. At 500 km, the smoothing due to the pre-processing using a Gaussian filter is more important and explains the slight increase of the absolute deviation as the spatial resolution is degraded. The

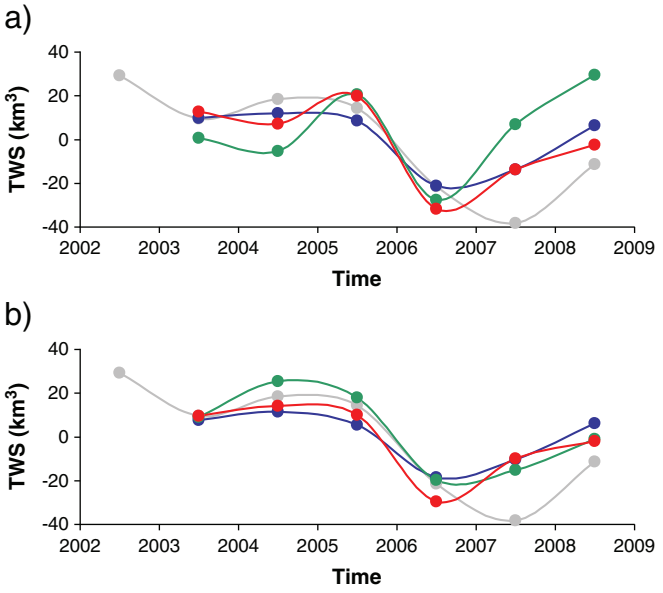

Fig. 14. Comparison of GRACE TWS annual anomalies with hydrological estimates from *in situ* measurements (SW and GW) and modeling (SM) for the period 2003–2008. The grey curves correspond to *in situ* + model TWS, the blue to ICA-filtered solutions, the green to Gaussian-filtered, and the red to destriped GFZ solutions at a) 400 km of filtering (300 km for the destriped solutions) and b) 500 km.

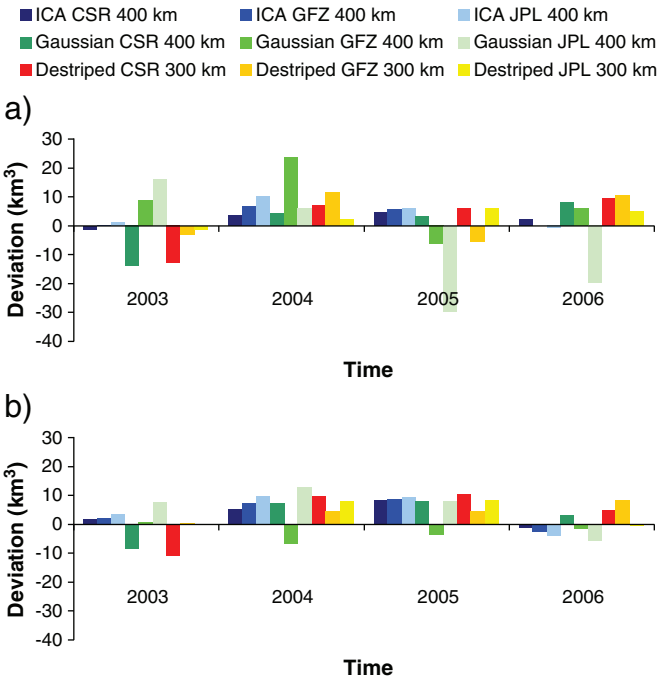

Fig. 15. Yearly deviation over 2003–2006 from *in situ* + model TWS of GRACE-derived TWS filtered with different approaches at a) 400 km of filtering (300 km for the destriped solutions) and b) 500 km. In blue, the ICA solutions (dark blue: CSR, blue: GFZ, and light blue: JPL), in green, the Gaussian solutions (dark green: CSR, green: GFZ, and light green: JPL), and the destriped and smoothed solutions (red: CSR, orange: GFZ, and yellow: JPL).

destriping method and the Gaussian filtering also exhibit good performances, even if important deviations are sometimes observed (particularly with the Gaussian filter for a radius of 400 km).

5. Conclusion

The ICA-based approach is a very efficient method for successfully separating TWS from noise in the GRACE Level-2 data. We demonstrated that this method is more robust than the classical filtering methods, such as the Gaussian filtering or the destriping. Comparisons at a global scale showed that the ICA-based solutions present less north–south stripes than Gaussian and destriped solutions on the land, and more realistic hydrological structures than the destriped solutions in the tropics. Trend maps over 2003–2008 have also been computed. The corresponding trend maps present more realistic trend patterns than those obtained with other types of solutions (see for example over the Amazon and Orinoco Basins with the 400 km radius of prefiltering). ICA filtering seems to allow the separation of the GIA from the TWS as negative trends were found over the Laurentides and Scandinavia. Unfortunately, this important geophysical parameter does not appear clearly in an ICA mode yet. The major drawback of this approach is that it cannot directly be applied to the GRACE Level-2 raw data, as a first step of prefiltering is required. In this study, we applied a Gaussian filtering which deteriorates the location of the important water mass patterns. This aspect of the pre-treatment to be improved and highlights the necessity to replace the Gaussian filter used for pre-processing the GRACE Level-2 raw data by one more suited to improve the quality of the GRACE-derived TWS and thus obtain trustworthy estimate of the trends.

At the basin-scale, the ICA-based solutions allowed us to filter out the unrealistic peaks present in the time series of TWS obtained using classical filtering for basins with areas lower than 1 million km². Among the ICA-based solutions, the JPL solutions are less affected by leakage compared with other solutions. JPL solutions also exhibit the lowest peak-to-peak amplitudes. The error balance of the GRACE-derived TWS is dominated by the effect of the leakage.

Validation with *in situ* measurements was performed in the Murray–Darling Basin where broad networks of *in situ* measurements of SW and GW are available. The ICA-based solutions are in better agreement with *in situ* data compared with the other types of solutions, especially where prefiltering at a 400 km of radius. The maximum deviations are lower by a factor two or three compared with the other filtering methods.

Acknowledgements

This work was partly supported by the Fondation Sciences et Techniques pour l'Aéronautique et l'Espace (STAE) in the framework of the CYMENT Project (post-doctoral grant for Frédéric Frappart) and the Australian Research Council grant DP0666300 (Marc Leblanc and Sarah Tweed). The authors also wish to thank Dr. Matthew Rodell for his help during the revision process.

References

Alsdorf, D. E., & Lettenmaier, D. P. (2003). Tracking fresh water from space. *Science*, *301*, 1492—1494.
Andersen, O. B., Seneviratne, S. I., Hinderer, J., & Viterbo, P. (2005). GRACE-derived terrestrial water storage depletion associated with the 2003 European heat wave. *Geophysical Research Letters*, *32*(18), L18405.
Bettadpur, S. (2007). CSR level-2 processing standards document for level-2 product release 0004, GRACE 327–742, Rev. 3.1.
Chambers, D. P. (2006). Evaluation of new GRACE time-variable gravity data over the ocean. *Geophysical Research Letters*, *33*, LI7603. doi:10.1029/2006GL027296
Chen, J. L., Wilson, C. R., Tapley, B. D., Yang, Z. L., & Niu, G. Y. (2009). 2005 drought event in the Amazon River basin as measured by GRACE and estimated by climate models. *Journal of Geophysical Research*, *114*, B05404. doi:10.1029/2008JB006056
Comon, P. (1994). Independent component analysis: A new concept? *Signal Processing*, *36*, 287—314.
Cresswell, R. G., Dawes, W. R., Summerell, G. K., & Walker, G. R. (2003). Assessment of salinity management options for Kyeamba Creek, New South Wales: Data analysis and groundwater modelling. *CSIRO Land and Water Technical Report 26/03*.
Cristescu, R., Joutsensalo, J., & Ristaniemi, T. (2000). Fading channel estimation by mutual information minimization for Gaussian stochastic processes. *Proceedings of IEEE International Conference on Communications (ICC2000), New Orleans, USA, June 18–22, 2000* (pp. 56—59).
CSIRO (2008). Water availability in the Loddon-Avoca. *A report to the Australian Government from the CSIRO Murray–Darling Basin Sustainable Yields Project*. Australia: CSIRO 123 pp.
Davis, J. L., Tamisiea, M. E., Elósegui, P., Mitrovica, J. X., & Hill, E. M. (2008). A statistical filtering approach for Gravity Recovery and Climate Experiment (GRACE) gravity data. *Journal of Geophysical Research*, *113*, B04410. doi:10.1029/2007JB005043
De Lathauwer, L., De Moor, B., & Vandewalle, J. (2000). An introduction to independent component analysis. *Journal of Chemometrics*, *14*, 123—149.
Ek, M. B., Mitchell, K. E., Lin, Y., Rogers, E., Grunmann, P., Koren, V., Gayno, G., & Tarpley, J. D. (2003). Implementation of Noah land surface model advances in the National Centers for Environmental Prediction operational mesoscale Eta model. *Journal of Geophysical Research*, *108*(D22), 8851. doi:10.1029/2002JD003296
Fetter, C. W. (2001). *Applied hydrogeology*, 4th ed. New Jersey: Prentice-Hall 598 pp.
Frappart, F., Papa, F., Famiglietti, J. S., Prigent, C., Rossow, W. B., & Seyler, F. (2008). Interannual variations of river water storage from a multiple satellite approach: A case study for the Rio Negro River basin. *Journal of Geophysical Research*, *113*, D21104. doi:10.1029/2007JD009438
Frappart, F., Ramillien, G., Biancamaria, S., Mognard, N. M., & Cazenave, A. (2006). Evolution of high-latitude snow mass derived from the GRACE gravimetry mission (2002–2004). *Geophysical Research Letters*, *33*, L02501.
Frappart, F., Ramillien, G. & Famiglietti, J. S. (in press). Water balance of the Arctic drainage system using GRACE gravimetry products. *International Journal of Remote Sensing*, doi:10.1080/01431160903474954
Frappart, F., Ramillien, G., Maisongrande, P., & Bonnet, M. -P. (2010). Denoising satellite gravity signals by independent component analysis. *IEEE Geosciences and Remote Sensing Letters*, *7*(3), 421—425. doi:10.1109/LGRS.2009.2037837
Gelle, G., Colas, M., & Serviere, C. (2001). Blind source separation: a tool for rotating machine monitoring by vibration analysis? *Journal of Sound and Vibration*, *248*, 865—885.
Han, S. -C., Shum, C. K., Jekeli, C., Kuo, C. -Y., Wilson, C., & Seo, K. -W. (2005). Non-isotropic filtering of GRACE temporal gravity for geophysical signal enhancement. *Geophysical Journal International*, *163*, 18—25.
Hekmeijer, P., & Dawes, W. (2003a). Assessment of salinity management options for South Loddon Plains, Victoria: Data analysis and groundwater modeling. *CSIRO Land and Water Technical Report 24/03*.

Hekmeijer, P., & Dawes, W. (2003b). Assessment of salinity management options for Axe Creek, Victoria: Data analysis and groundwater modelling. *CSIRO Land and Water Technical Report 22/03, MDBC Publication 08/03* 40 pp.

Hyvärinen, A. (1999). Fast and robust fixed-point algorithms for independent component analysis. *IEEE Transactions on Neural Networks*, *10*, 626−634.

Hyvärinen, A., & Oja, E. (2000). Independent component analysis: algorithms and applications. *Neural Networks*, *13*, 411−430.

Ife, D. and Skelt, K. (2004). Murray–Darling Basin Groundwater Status 1990–2000. Murray–Darling Basin Commission, publication 32/04, Canberra. ISBN 1876830948. Available online at http://www.mdbc.gov.au

Jekeli, C. (1981). Alternative methods to smooth the Earth's gravity field. *Tech. Rep., Department of Geodetic Science, Ohio State University, Colombus, Ohio*.

Kirby, M., Evans, R., Walker, G., Cresswell, R., Coram, J., Khan, S., Paydar, Z., Mainuddin, M., McKenzie, N. and Ryan, S. (2006). The shared water resources of the Murray–Darling Basin. Murray–Darling Basin Commission, Publication 21/06, Canberra. ISBN 192103887X. Available online at http://www.mdbc.gov.au

Klees, R., Revtova, E. A., Gunter, B. C., Ditmar, P., Oudman, E., Winsemius, H. C., & Savenije, H. H. G. (2008). The design of an optimal filter for monthly GRACE gravity models. *Geophysical Journal International*, *175*, 417−432. doi:10.1111/j.1365-246X.2008.03922.x

Kusche, J. (2007). Approximate decorrelation and non-isotropic smoothing of time-variable GRACE-type gravity field models. *Journal of Geodesy*, *81*, 733−749.

Lawrence, J. E., & Hornberger, G. M. (2007). Soil moisture variability across climate zones. *Geophysical Research Letters*, *34*, L20402. doi:10.1029/2007GL031382

Leblanc, M. J., Tregoning, P., Ramillien, G., Tweed, S. O., & Fakes, A. (2009). Basin-scale, integrated observations of the early 21st century multiyear drought in southeast Australia. *Water Resources Research*, *45*, W04408. doi:10.1029/2008WR007333

Macumber, P. G. (1999). *Groundwater flow and resource potential in the Bridgewater and Salisbury West GMAs*.Melbourne: Phillip Macumber Consulting Services 88 pp.

Oki, T., & Sud, Y. C. (1998). Design of Total Runoff Integrating Pathways (TRIP) — A global river channel network. *Earth Interactions*, *2*(1), 1−37.

Paulson, A., Zhong, S., & Wahr, J. (2007). Inference of mantle viscosity from GRACE and relative sea level data. *Geophysical Journal International*, *171*(2), 497−508.

Peltier, W. R. (2004). Global glacial isostasy and the surface of the ice-age earth: The ICE-5G(VM2) model and GRACE. *Annual Review of Earth and Planetary Sciences*, *32*, 111−149.

Petheram, C., Dawes, W., Walker, G., & Grayson, R. B. (2003). Testing in class variability of groundwater systems: Local upland systems. *Hydrological Processes*, *17*, 2297−2313.

Pöyhönen, S., Jover, P., & Hyötyeniemi, H. (2003). Independent component analysis of vibrations for fault diagnosis of an induction motor. *Proceedings of the IASTED International Conference on Circuits, Signal and Systems (CSS 2003), Cancun, Mexico, 19–21 May 2003, 1*. (pp. 203−208).

Ramillien, G., Famiglietti, J. S., & Wahr, J. (2008). Detection of continental hydrology and glaciology signals from GRACE: A review. *Surveys in Geophysics*, *29*, 361−374. doi:10.1007/s10712-008-9048-9

Ramillien, G., Frappart, F., Cazenave, A., & Güntner, A. (2005). Time variations of land water storage from the inversion of 2-years of GRACE geoids. *Earth and Planetary Science Letters*, *235*, 283−301. doi:10.1016/j.epsl.2005.04.005

Ramillien, G., Frappart, F., Güntner, A., Ngo-Duc, T., Cazenave, A., & Laval, K. (2006). Time-variations of the regional evapotranspiration rate from Gravimetry Recovery And Climate Experiment (GRACE) satellite gravimetry. *Water Resources Research*, *42*, W10403. doi:10.1029/2005WR004331

Ramillien, G., Lombard, A., Cazenave, A., Ivins, E. R., Llubes, M., Remy, F., & Biancale, R. (2006). Interannual variations of the mass balance of the Antarctica and Greenland ice sheets from GRACE. *Global and Planetary Change*, *53*(3), 198−208.

Ristaniemi, T., & Joutsensalo, J. (1999). On the performance of blind symbol separation in CDMA downlink. *Proceedings of the International Workshop on Independent Component Analysis and Signal Separation (ICA'99), Aussois, France, January 11–15, 1999* (pp. 437−442).

Rodell, M., Chen, J., Kato, H., Famiglietti, J. S., Nigro, J., & Wilson, C. (2007). Estimating groundwater storage changes in the Mississippi River basin (USA) using GRACE. *Hydrogeology Journal*, *15*(1), 159−166.

Rodell, M., Famiglietti, J. S., Chen, J., Seneviratne, S. I., Viterbo, P., Holl, S., & Wilson, C. R. (2004). Basin scale estimates of evapotranspiration using GRACE and other observations. *Geophysical Research Letters*, *31*(20), L20504.

Rodell, M., Houser, P. R., Jambor, U., & Gottschalck, J. (2004). The Global Land Data Assimilation System. *Bulletin of the American Meteorological Society*, *85*(3), 381−394. doi:10.1175/BAMS-85-3-381

Sasgen, I., Martinec, Z., & Fleming, K. (2006). Wiener optimal filtering of GRACE data. *Studia Geophysica et Geodaetica*, *50*, 499−508.

Schmidt, R., Flechtner, F., Meyer, U., Neumayer, K. -H., Dahle, Ch., Koenig, R., & Kusche, J. (2008). Hydrological signals observed by the GRACE satellites. *Surveys in Geophysics*, *29*, 319−334. doi:10.1007/s10712-008-9033-3

Seitz, F., Schmidt, M., & Shum, C. K. (2008). Signals of extreme weather conditions in Central Europe in GRACE 4-D hydrological mass variations. *Earth and Planetary Science Letters*, *268*(1–2), 165−170.

Seo, K. -W., & Wilson, C. R. (2005). Simulated estimation of hydrological loads from GRACE. *Journal of Geodesy*, *78*, 442−456.

Smitt, C., Doherty, J., Dawes, W., & Walker, G. (2003). Assessment of salinity management options for the Brymaroo catchment, South-eastern Queensland. *CSIRO Land and Water Technical Report 23/03*.

Stone, J. V. (2004). *Independent component analysis: A tutorial introduction.* : MIT Press: Bradford Book.

Strassberg, G., Scanlon, B. R., & Rodell, M. (2007). Comparison of seasonal terrestrial water storage variations from GRACE with groundwater-level measurements from the High Plains Aquifer (USA). *Geophysical Research Letters*, *34*, L14402. doi:10.1029/2007GL030139

Swenson, S., & Wahr, J. (2006). Post-processing removal of correlated errors in GRACE data. *Geophysical Research Letters*, *33*, L08402. doi:10.1029/2005GL025285

Syed, T. H., Famiglietti, J. S., & Chambers, D. (2009). GRACE-based estimates of terrestrial freshwater discharge from basin to continental scales. *Journal of Hydrometeorology*, *10*(1). doi:10.1175/2008JHM993.1

Tapley, B. D., Bettadpur, S., Ries, J. C., Thompson, P. F., & Watkins, M. (2004). GRACE measurements of mass variability in the Earth system. *Science*, *305*, 503−505.

Urbano, L. D., Person, M., Kelts, K., & Hanor, J. S. (2004). Transient groundwater impacts on the development of paleoclimatic lake records in semi-arid environments. *Geofluids*, *4*, 187−196.

van Hateren, J. H., & van der Schaaf, A. (1998). Independent component filters of natural images compared with simple cells in primary visual cortex. *Proceedings of the Biological Society*, *265*, 359−366.

Vigário, R. (1997). Extraction of ocular artifacts from EEG using independent component analysis. *Encephalography and Clinical Neurophysiology*, *103*(3), 395−404.